J Mater Sci (2007) 42:8707–8713
DOI 10.1007/s10853-007-1739-y

Fabrication of conductive $SrRuO_3$ thin film and $Ba_{0.60}Sr_{0.40}TiO_3$/$SrRuO_3$ bilayer films on MgO substrate

Wen Feng Qin · Wan Yong Ai · Jun Zhu · Jie Xiong · Jinlong Tang · Ying Zhang · Yan Rong Li

Received: 5 February 2007 / Accepted: 2 April 2007 / Published online: 18 July 2007

Abstract Conductive $SrRuO_3$ (SRO) thin films have been grown on (100) MgO substrates by pulsed laser deposition (PLD) technique. Effects of oxygen pressure and deposition temperature on the orientation of SRO thin film were investigated. X-ray diffraction (XRD) $\theta/2\theta$ patterns and the temperature dependent resistivity measurements indicated that oxygen pressure of 30 Pa and deposition temperature of 700 °C were the optimized deposition parameters. A parallel-plate capacitor structure was prepared with the SRO films deposited under optimized condition as an electrode layer and $Ba_{0.60}Sr_{0.40}TiO_3$ (BST) thin film as the dielectric layer. XRD Φ scans indicated a [001]BST//$[110/001]SRO//[001]MgO$ epitaxial relationship between BST and SRO on MgO substrate. The dielectric constant and loss tangent measured at 10 kHz and 300 K was 427 and 0.099 under 0 V bias, and 215 and 0.062 under 8 V bias, respectively. A tunability of 49.6% has been achieved with DC bias as low as 8 V. The *C–V* hysteresis curve and the *P–E* hysteresis loop suggested that the BST films epitaxially grown on SRO/MgO have ferroelectricity at room temperature. The induced ferroelectricity was believed to originate from the compressive strain between the epitaxial BST and SRO thin films. These results show the potential application of the BST/SRO heterostructures in microelectronic devices.

W. F. Qin (✉) · W. Y. Ai · J. Zhu · J. Xiong · J. Tang · Y. Zhang · Y. R. Li
State Key Laboratory of Electronic Thin Films and Integrated Devices, University of Electronics Science and Technology of China, Chengdu 610054, China
e-mail: qinhaochen2006@hotmail.com

Introduction

Perovskite oxide thin films have been found to be important to scientific studies and technological applications since these materials exhibit a wide range of properties and phenomena ranging from insulting to semiconducting and superconducting; from paramagnetic to ferromagnetic; and from paraelectric to ferroelectric [1]. Among a large range of perovskite oxide materials, the conductive metallic oxide $SrRuO_3$(SRO) has been extensively investigated recently due to their important electrical and magnetic properties and potential applications in a number of different fields [2]. $SrRuO_3$ is an ideal bottom electrode in devices incorporating oriented ferroelectric films due to its outstanding thermal conductivity and stability, high resistance to chemical erosion, and good compatibility in structure with perovskite type ferroelectric materials [3]. (Pb,Zr)TiO_3 ferroelectric and (Ba,Sr)TiO_3 high dielectric constant capacitors with $SrRuO_3$ thin film electrodes exhibit superior fatigue and low leakage characteristics [4, 5].

It is reported that $SrRuO_3$ has a pseudo-cubic perovskite structure, which is distorted from the ideal cubic perovskite structure by tilting the RuO_6 octahedral [6]. At room temperature, it is an orthorhombic phase with the space group of Pbnm (No. 62) and lattice parameters a = 5.5670 Å, b = 5.5304 Å, and c = 7.8446 Å which can be described as a slightly distorted pseudo-cubic perovskite cell with a_c = 3.93 Å [7]. It should be pointed out that all the planes and directions of $SrRuO_3$ referred to in this work are based on the orthorhombic unit cell. Due to a good lattice match, the majority of epitaxial $SrRuO_3$ thin films have been grown on $SrTiO_3$ or $LaAlO_3$ single-crystal substrates by various deposition methods. When $SrRuO_3$ is deposited on a (001) $SrTiO_3$ or (001) $LaAlO_3$ substrate, the orthorhombic symmetry of the $SrRuO_3$ unit cell is

preserved. The film can be grown with its (001), (110) or ($1\bar{1}0$) planes parallel to the substrate surface [8], and they exhibited six possible domain structure and orientation.

The $Ba_xSr_{1-x}TiO_3$ (BST) system, which takes advantage of the high dielectric constant of $BaTiO_3$ and the structural stability of $SrTiO_3$ [9], has become very attractive to the microelectronic industry as good candidates for application in high-density dynamic random access memories (DRAM) and tunable microwave devices due to its outstanding dielectric properties [10]. The fabrication of high-quality $Ba_xSr_{1-x}TiO_3$ films exhibiting high ε_r, low tanδ, and low J_L values has become a very important technological issue for pushing these materials further into practical applications [11].

To our best knowledge, there have been few reports of the growth of $SrRuO_3$ on MgO substrates and little work has been done with respect to the combination of BST/SRO that shows excellent electrical properties. In this work, we report the growth of $SrRuO_3$ thin films on MgO substrates under different process parameters. Then a BST based parallel-plate capacitor structure was prepared with conductive SRO thin film electrode layer deposited under optimized conditions. High quality $SrRuO_3$ thin films can be epitaxially grown on MgO substrates under the proper deposition conditions and they can serve as a promising candidate of electrode materials for the fabrication of BST thin films with good electrical properties.

Experimental

Two groups of starting powders ($BaCO_3$, $SrCO_3$, TiO_2 and $SrCO_3$, RuO_2) with the composition ratio of Ba/Sr = 60/40 and Sr/Ru = 1 were mixed for 24 h using agate ball miller. Mixed powders were pressed to form BST and SRO targets, which were subsequently sintered in air for 3 h at 1,350 and 1,550 °C, respectively.

$SrRuO_3$ thin films were deposited on (100) MgO single-crystal substrates using a pulse laser deposition (PLD) technique. During growth, the target was rotated and the laser beam was scanned across the target surface to minimize degradation [12]. A pulsed KrF excimer laser (λ = 248 nm) with a repetition rate of 3 Hz was employed for the deposition. The laser beam was focused onto the target with a fluence of about 2 J/cm^2 at an angle of 45°. The substrate was placed parallel to the target at a distance of about 5 cm. The films were deposited at various oxygen pressure from 10 Pa to 50 Pa and at a temperature range of 600–700 °C. After deposition, 0.5 atm high-purity oxygen was introduced into the growth chamber, and the grown films were annealed at 500 °C for 10 min and then cooled to room temperature. The thickness of the films was determined to be about 100 nm by step profile.

The crystallinity and the structure of $SrRuO_3$ films deposited at different oxygen pressure and different temperature was characterized by X-ray diffraction (XRD) with Cu Kα radiation (D1 System, Bede). The room temperature electrical resistivity was tested by the classical four-probe measurement. Atomic force microscopy (AFM)(SPA-300HV, Seiko) was employed to investigate the morphology of the thin films. The optimized process parameters for epitaxial SRO thin films on MgO substrate were obtained from the above results.

A parallel-plate capacitor structure was prepared with the SRO films deposited under optimized condition as an electrode layer and $Ba_{0.60}Sr_{0.40}TiO_3$ as the dielectric layer. The BST thin films with thickness of about 200 nm was deposited on SRO/MgO at 30 Pa oxygen ambient and at a temperature of 650 °C. For dielectric property measurements, Au circular dots of diameter 0.4 mm were deposited by DC magnetron sputtering through a shadow mask to form a metal-insulator-metallic oxide (MIM) configuration. The capacitance and dielectric loss were measured using HP 4284 impedance analyzer. The *P–E* hysteresis loop measurement was carried out with a TF Analyzer 2000 standardized ferroelectric test system. The dielectric constant of the BST thin films was calculated from the capacitance using the following equation:

$$\varepsilon_r = Cd/\varepsilon_0 A,$$

where C is the capacitance, ε_0 the free space dielectric constant value ($8.85*10^{-12}$F/m), A the capacitor area (m^2) and d (m) the thickness of the BST films.

Results and discussion

Figure 1 shows the XRD patterns of SRO thin films on MgO substrates deposited by PLD at a temperature of 650 °C and at oxygen pressure of 10, 30, and 50 Pa, respectively. In the XRD $\theta/2\theta$ patterns, the two peaks located at 22° and 46° can be indexed as SRO (110) or (002) and SRO (220) or (004). Because of the systematic absence of the (0,0,l) peaks, where l is odd, and the near degeneracy of the d_{110} and d_{002} in $SrRuO_3$ (d is the inter planar spacing), it is not possible to distinguish between these two textures using a simple 2θ scan [12]. As revealed by the XRD patterns, SRO films deposited at 30 Pa oxygen pressures shows a good out-plane orientation. Increasing or decreasing the oxygen pressure would result in a worse out-plane orientation. Especially when the oxygen pressure was increased to 50 Pa, the obtained SRO films were not crystallized. This is properly because the increasing of the oxygen pressure would result in losing of kinetic energy of the ablated species by random collisions with atoms or

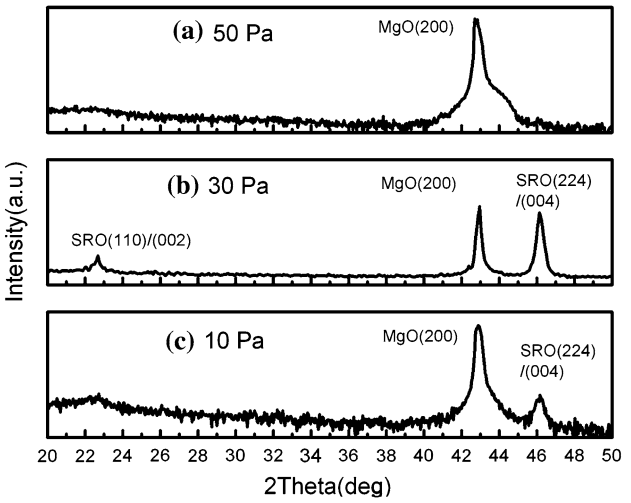

Fig. 1 XRD patterns of SRO films deposited at temperature 650 °C and pressure (**a**) 50 Pa, (**b**) 30 Pa and (**c**) 10 Pa

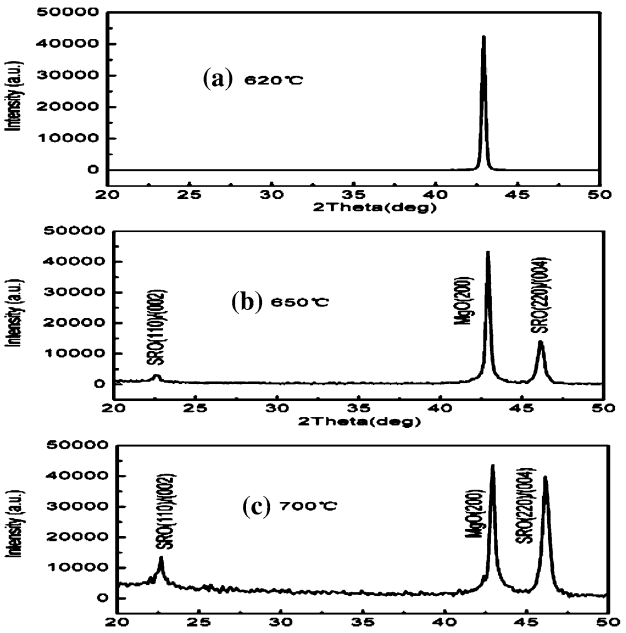

Fig. 2 XRD patterns of SRO films deposited at oxygen pressure 30 Pa and at different temperatures (**a**) 620 °C, (b) 650 °C and (**c**) 700 °C

molecules of the background gas. In contrast, less oxygen cannot meet the demand of the formation of stable crystalline structure for SRO at lower pressure of 10 Pa. So oxygen pressure of 30 Pa could be a proper condition for deposition of SRO thin films.

As we know, in the application of SRO oxide electrodes to electric devices, such as MIM (Metal-insulator-metallic)capacitors and MISFETs (metal-insulator-semiconductor field-effect transistors), the interface diffusion which occurs easily at high temperature as well as high conductivity has been the central subject. So far, SRO thin films grown at high temperatures, e.g. 750–800 °C, have been reported to show high quality. Fabrication of SRO thin films at a relatively lower temperature with acceptable film quality reveals a means of solving the interface diffusion problem. In this work, we attempt to grow SRO thin films with acceptable structural and electrical properties at low temperatures. Investigation of structural and electrical properties of SRO thin films grown at various temperatures ranging from 600 °C to 700 °C is presented here. Figure 2 shows the XRD patterns of SRO thin films on MgO substrates deposited at 30 Pa and at different growth temperatures. As can be seen in Fig. 2, the crystal orientation and crystallinity of the SRO films are strongly dependent on the growth temperature. It was found that amorphous films were obtained for growth temperature below 650 °C while crystalline films were obtained at the growth temperature of 650 °C or higher. By the comparison of intensity of the major peaks, it can be deduced that the crystallinity increase with increasing growth temperature. The dependence of the room temperature resistivity of SRO film on deposition temperature is shown in Fig. 3. The value of resistivity of SRO thin films decreases as the deposition temperature increases, indicating that better conductivity is achieved when films are deposited at higher temperatures. As is clearly shown in Fig. 3, the resistivity decreases abruptly when the temperature is above 650 °C, indicating its excellent crystallinity, which was consist with the XRD result shown in Fig. 2. The room temperature resistivity of $SrRuO_3$ films deposited at a temperature of 650 and 700 °C was about 500 and 300 $\mu\Omega$ cm, respectively. Jia et al. reported that the room-temperature resistivity of SRO films on LAO was about 280 $\mu\Omega$ cm at a deposition temperature

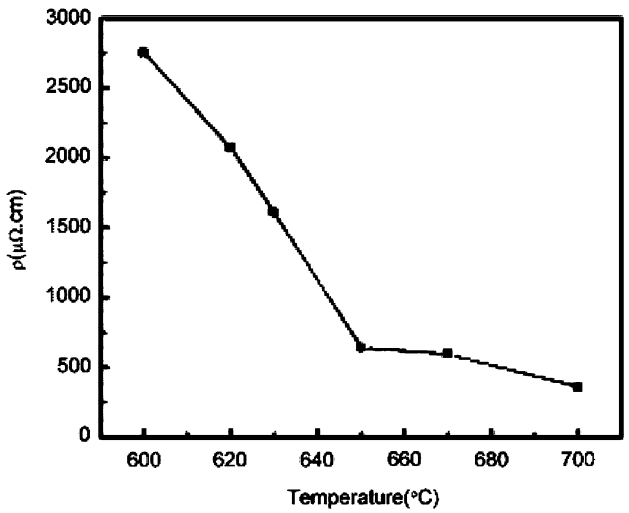

Fig. 3 The variation of the room temperature resistivity of SRO film as a function of deposition temperature

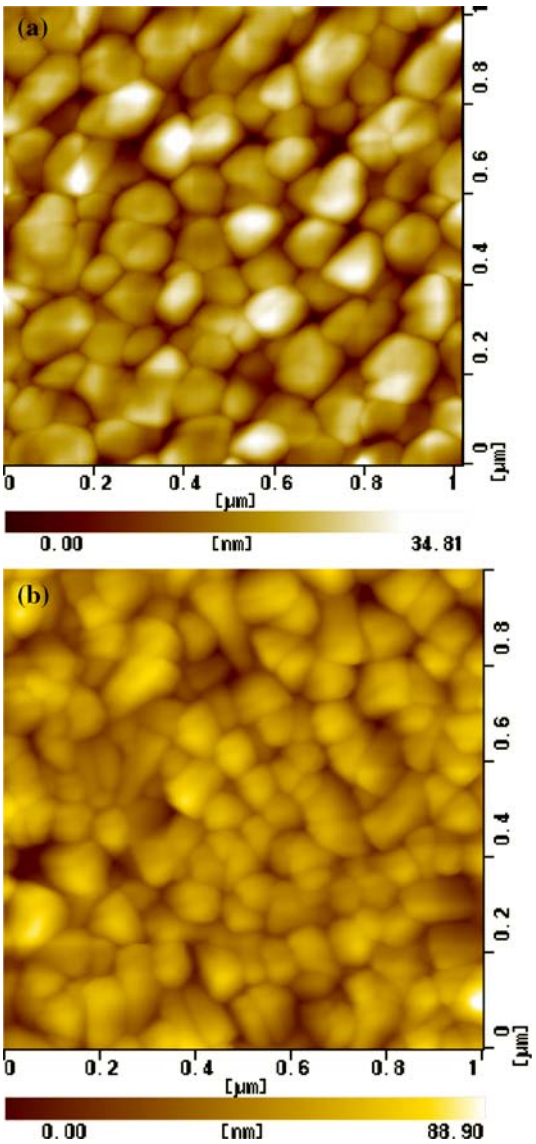

Fig. 4 AFM surface images over 1×1 μm^2 for (**a**) 100 nm SrRuO3 film on MgO substrate and (**b**) 200 nm BST film on SRO/MgO

of 775 °C [2]. Chen et al. reported a room-temperature resistivity of 310 $\mu\Omega$ cm for SRO films deposited on STO [1]. The value of resistivity of SRO on MgO at 700 °C is quite comparable to that on STO and LAO, indicating the potential application of SRO/MgO for electrode layer.

Recently, $Ba_xSr_{1-x}TiO_3$, a high permittivity material, is recognized to be a potential capacitor dielectric film for microelectronic circuits. To fabricate high performance BST thin film capacitors, a proper bottom electrode has to be utilized. The conductive metallic oxide SRO has the same crystal structure, perovskite-type, as BST and its lattice constant are similar to that of BST. Furthermore, SRO has high chemical and thermal stability, which are very important to realize the integration between high dielectric materials and active devices located on the substrates. It was found that (Ba,Sr)TiO_3 high dielectric constant capacitors with $SrRuO_3$ thin film electrodes exhibit improved dielectric properties and superior fatigue and low leakage characteristics [4, 5].

From the above results, we can conclude that the optimized condition for fabricating SRO thin films on MgO substrates is at the oxygen pressure of 30 Pa and at the deposition temperature of 700 °C. The SRO thin film deposited under optimized condition shows a dense and smooth surface with a root-mean-square(RMS) roughness of 6.1 nm over a 1×1 μm^2 scan area, as shown in Fig. 4a. A smooth surface is necessary for the electrode application because hillocks on the surface of the electrode layer can electrically short the capacitors. To verify the quality of the as-grown SRO thin films and their potential application, BST thin films with thickness of about 200 nm was deposited on SRO/MgO at 30 Pa oxygen ambient and at a temperature of 650 °C by PLD to form a parallel-plate capacitor. The surface morphology of the BST film deposited on SRO/MgO is shown in Fig. 4b. The AFM micrograph reveals that the BST film is well-crystallized and crack free. The RMS roughness over the 1×1 μm^2 surface is 14 nm.

The epitaxial nature of both BST and SRO films were demonstrated by the in-plane orientation with respect to the major axis of the substrate. Figure 5 shows the XRD Φ-scan on (101) BST, (224) SRO, (204) SRO and (202) MgO, respectively. Figure 5b shows four peaks separated by 90° from each other which indicates the coexistence of two (110)-type domains. The in-plane orientation relationship was deduced to be SRO[001]//MgO[010] and SRO[1-10]//MgO[001] (mode X), or SRO[001]//MgO[001] and SRO[-110]//MgO[010] (mode Y). However, the Φ scan of SRO(204) as shown in Fig. 5c shows four peaks which demonstrates that the coexistence of two (001)-type domain. The (204) peaks of $SrRuO_3$ thin films with the perovskite structure are shifted 45° with respect to the (202) peaks of MgO substrate. This indicates that the perovskite compound rotated 45° with respect to the structure of MgO crystal. The in-plane orientation relationship was deduced to be either SRO[100]//MgO[011] and SRO[010]//MgO[$0\bar{1}1$] (mode Z), or SRO[010]//MgO[011] and SRO[100]//MgO[$01\bar{1}$] (mode Z′). Figure 6 shows a schematic diagram of this domain structure of $SrRuO_3$ film on MgO substrate as deduced from the XRD data. This domain structure of SRO thin film on MgO substrate is in agreement with the result of Jiang [13], in which the SRO thin film grown on LAO substrate shows similar domain structure. As discussed above, SRO is pseudo-cubic with slight orthorhombic distortion. The orthorhombic unit cell is oriented such that its [110] direction corresponds to the [100] direction of the pseudo-cubic

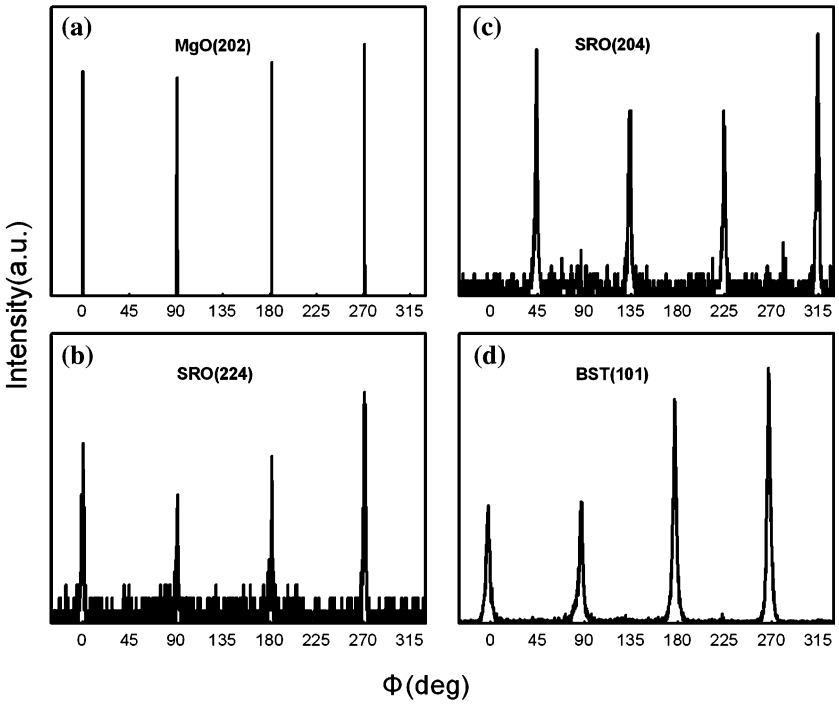

Fig. 5 In plane Φ scan of (**a**) MgO (202), (**b**) SRO (224), (**c**) SRO (204) and (**d**) BST (101)

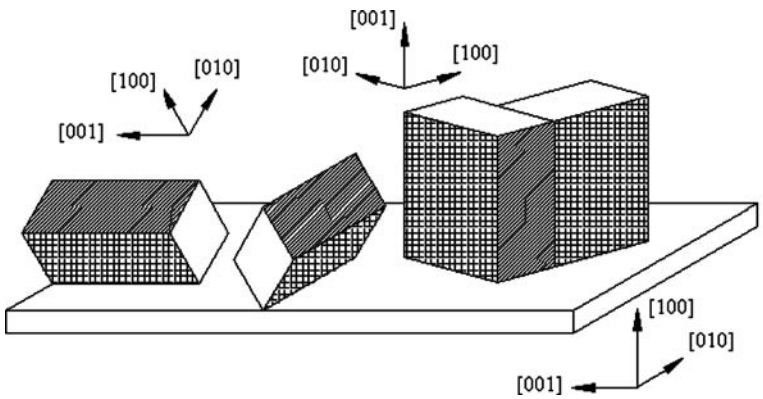

Fig. 6 Schematic diagram of domain structure of $SrRuO_3$ film on MgO substrate

cell, while the *c*-axis of the orthorhombic and pseudo-cubic cells are parallel [14]. When the $SrRuO_3$ thin films grow with the orthorhombic [110] axis normal to the substrate and the *c*-axis in plane, the corresponding pseudo-cubic cell sits cube-on-cube with the underlying cubic substrate lattice. When the films grow with *c*-axis normal to the substrate, it would also result in a cube-on-cube arrangement of the pseudo-cubic $SrRuO_3$ cell and cubic substrate lattice. So the six possible domain structure of SRO thin film all correspond to a cube-on-cube arrangement with respect to the substrate. So this multi-domain structure of SRO bottom electrode would not affect the microstructure of BST thin films deposited on SRO. The XRD Φ-scan on (101) BST, given in Fig. 5d, shows four peaks separated by 90° from each other indicating the *c*-orientation of BST film. This is in agreement with the XRD $\theta/2\theta$ pattern of BST/SRO/MgO which is not shown here. So [001] BST is //[001] MgO via two SRO out-plane orientations: [110] SRO// [001] STO and 45°-rotated cube-on-cube [001] SRO// [001] STO, which are formed by two in-plane arrangements each as analyzed above. This growth pattern is quite reasonable by considering the lattice parameters for each of the materials (MgO: $a = b = c = 4.21$ Å; SRO: $a = 5.5670$ Å, $b = 5.5304$ Å, and $c = 7.8446$ Å; and BST: $a = b = 3.97$ Å, $c = 3.98$ Å). This growth pattern will give a minimum lattice mismatch between the layers of BST/SRO and SRO/MgO.

Dielectric properties of the BST films were obtained through the investigation of capacitor with a configuration of Au/BST/SRO. The room temperature capacitance–

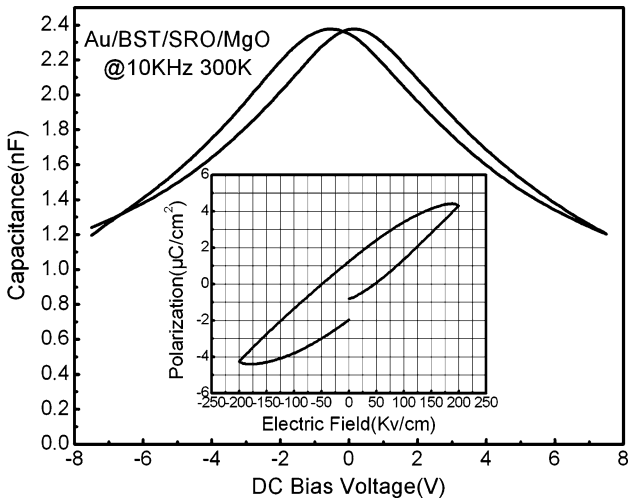

Fig. 7 Dielectric constant as a function of applied DC bias voltage for the BST thin film. The inset shows the *P–E* hysteresis loop

voltage (*C–V*) curve of the parallel-plate capacitor was shown in Fig. 7, which was measured at the frequency of 10 kHz with a small AC signal amplitude of 100 mV, while the DC bias voltage was swept cyclically from negative bias (–8 V) to positive bias (+8 V) at a sweep rate of 0.2 V/s and then back. In the case of the sample measured here, the values of the relative dielectric constant, ε_r, and loss tangent, tanδ, of 427 and 0.099 under no bias, and 215 and 0.062 under 8 V bias, respectively, were achieved. A tunability of 49.6% has been achieved with DC bias as low as 8 V. During the two scanning process, the capacitance showed two peaks with increasing and decreasing applied voltage. From the *C–V* hysteresis curve, it can be concluded that BST films which was epitaxially grown on SRO/MgO, have ferroelectricity at room temperature. The *P–E* hysteresis shown in the inset of Fig. 8 further

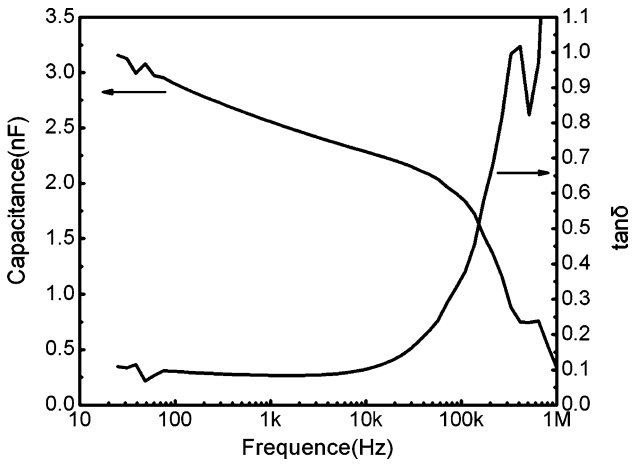

Fig. 8 Frequency dependence of dielectric constant and dielectric loss of the BST thin-film

confirmed this. According to the measurements, the coercive field (E_c) and the remnant polarization (P_r) of BST films were 50 kV/cm^2 and 2.0 μC/cm^2, respectively. Abe et al. reported that epitaxially grown BST thin films with Ba content $x \geq 0.44$ on Pt/MgO had ferroelectricity at room temperature [15]. Sinnamon et al. reported a strain-induced stabilization of ferroelectricity in SRO/BST/Au thin films capacitors [16]. Our result of ferroelectricity for epitaxial BST film on SRO-coated MgO is also attributed to the induction effect of interface. The induced ferroelectricity was believed to be in relation to the elongated lattice constant of BST in the thickness direction, which probably originate from the compressive strain between BST and SRO, since the lattice constant of SRO is smaller than that of BST.

The frequency dependence of the capacitance and tanδ is shown in Fig. 8.The ε_r decrease from around 568 to 411 with increasing frequency from 20 Hz to 10 kHz. The tanδ, which shows a minimum value at a frequency around 10 kHz, is about 0.06. The typical leakage current density is about 8×10^{-7} A/cm^2 at a field intensity of 200 kV/cm. The good electrical and dielectric properties of BST films on SRO-coated MgO in our case, compared to those of epitaxial BST with Pt and $YBa_2Cu_3O_{7-x}$ as a bottom electrode [17], is believed to originate from the better structural perfection of the BST films by using SRO as a bottom electrode.

Conclusion

In conclusion, high quality $SrRuO_3$ thin films have been successfully epitaxially grown on single crystal MgO substrates by PLD in 30 Pa oxygen ambient and at a temperature of above 650 °C. The room temperature resistivity of $SrRuO_3$ films deposited at a temperature of 700 °C was 300 $\mu\Omega$ cm. $Ba_{0.60}Sr_{0.40}TiO_3$ (BST) thin film has been deposited on this SRO/MgO electrode layer to form a SRO/BST/Au thin film capacitor. XRD Φ scans indicated a [001]BST//[110/001]SRO//[001]MgO epitaxial relationship between BST and $SrRuO_3$ on MgO substrate. The dielectric constant and loss tangent measured at 10 kHz and 300 K were 427 and 0.099 under no bias, and 215 and 0.062 under 8 V bias, respectively. A tunability of 49.6% has been achieved with DC bias as low as 8 V. The *C–V* hysteresis curve and the *P–E* hysteresis loop indicated that the BST films which was epitaxially grown on SRO/MgO, have ferroelectricity at room temperature. The induced ferroelectricity was believed to originate from the compressive strain between the epitaxial BST and SRO thin films. These results show the potential of the BST/SRO heterostructures for microelectronic device application.

References

1. Chen CL, Cao Y, Huang ZJ, Jiang QD, Zhang Z, Sun YY, Kang WN (1997) Appl Phys Lett 71(8):1047
2. Jia QX, Foltyn SR, Hawley M, Wu XD (1997) J Vac Sci Technol A 15(3):1080
3. Singh SK, Lees MR, Singh RK, Palmer SB (2002) J Phys D: Appl Phys 35:2243–2246
4. Jiang JC, Tian W, Pan XQ (1998) Appl Phys Lett 72:2963
5. Fang X, Kobayashi T (2001) J Appl Phys 90:162
6. Gausepohl SC, Lee M, Rao RA, Eom CB (1996) Phys Rev B 54:8996
7. Vasco E, Dittmann R, Karthaüser S, Waser R (2003) Appl Phys Lett 82:2497
8. Herranz G, Sánchez F, Fontcuberta J (2005) Phys Rev B 71:174411
9. Syamaprasad U, Galgali RK, Mohanty BC (1989) Mater Lett 8:36
10. Yang G, Gu HS, Zhu J, Wang YQ (2002) J Crystal Growth 242:172
11. Zhu XH et al (2004) J Cryst Growth 268:192
12. Singh SK, Lees MR, Singh RK, Palmer SB (2002) J Phys D: Appl Phys 35:2243
13. Jiang JC, Pan XQ (2001) J Appl Phys 89:6365
14. Kennedy RJ, Madden R, Stampe PA (2001) J Phys D: Appl Phys 34:1853
15. Abe K, Komatsu S (1995) J Appl Phys 77:6461
16. Sinnamon LJ, Bowman RM, Gregg JM (2002) Appl Phys Lett 81:889
17. Yoon S-G, Lee J-C, Safari A (1994) J Appl Phys 76:2999